Separation Science and Technology

ISSN: (Print) (Online) Journal homepage: https://www.tandfonline.com/loi/lsst20

Investigating the effects of sacrificial agents on MO dye degradation with Ag_2Se nanocomposites via chemical wet method using visible light irradiation

Hassan Akbar, Alishba Zulfiqar, Hijab Imran, Ali Raza, Faiza Anjum, Syeda Tehreem Iqbal, Ashfaq Ahmad & Asghar Ali

To cite this article: Hassan Akbar, Alishba Zulfiqar, Hijab Imran, Ali Raza, Faiza Anjum, Syeda Tehreem Iqbal, Ashfaq Ahmad & Asghar Ali (2023): Investigating the effects of sacrificial agents on MO dye degradation with Ag_2Se nanocomposites via chemical wet method using visible light irradiation, Separation Science and Technology, DOI: 10.1080/01496395.2023.2252585

To link to this article: https://doi.org/10.1080/01496395.2023.2252585

Published online: 28 Aug 2023.

SEPARATION SCIENCE AND TECHNOLOGY
https://doi.org/10.1080/01496395.2023.2252585

Taylor & Francis
Taylor & Francis Group

Investigating the effects of sacrificial agents on MO dye degradation with Ag_2Se nanocomposites via chemical wet method using visible light irradiation

Hassan Akbar[a,b], Alishba Zulfiqar[c], Hijab Imran[c], Ali Raza[c], Faiza Anjum[c], Syeda Tehreem Iqbal[c], Ashfaq Ahmad[d], and Asghar Ali[c]

[a]Department of Physics, Abbottabad University of Science and Technology (AUST), Abbottabad, Pakistan; [b]College of Environmental Science and Engineering, North China Electric Power University, Beijing, China; [c]Department of Physics, The University of Lahore, Lahore, Pakistan; [d]School of Material Science and Engineering, Shanghai Jiaotong University, Shanghai, China

ABSTRACT

In this study, the degradation of MO (Methyl orange) dye using visible light irradiation and Ag_2Se photo-catalyst was investigated. The Ag_2Se photo-catalyst was synthesized via a wet chemical technique and characterized by using X-ray diffraction (XRD) for structural analysis, scanning electron microscopy (SEM) for surface morphology, transmission electron microscopy (TEM) for inner structure, Raman and UV-Vis spectroscopy for the study of its optical properties. The results showed that the Ag_2Se photo-catalyst has a well-defined cubic crystal structure with a typical particle size of 50 to 76.5 nm. The UV-Vis absorption spectrum of the Ag_2Se photo-catalyst revealed a strong absorption in the visible light region, indicating its potential as visible light photo-catalyst. The photocatalytic degradation of MO dye was carried out under visible light irradiation using the synthesized Ag_2Se photo-catalyst. The results showed that the degradation efficiency of MO dye reached 95% after 150 min of irradiation. The degradation of MO dye was attributed to the generation of reactive oxygen species (ROS) and the formation of Ag nanoclusters on the surface of the Ag_2Se photo-catalyst. The stability of the Ag_2Se photo-catalyst was also examined, and the results exhibited that the photo-catalyst was stable and could be reused for subsequent photo-catalytic degradation experiments. The Ag_2Se photo-catalyst showed an outstanding photo catalytic activity for the degradation of MO dye underneath visible light irradiation. The study proposes that the Ag_2Se photo-catalyst can be used for the treatment of wastewater containing organic pollutants.

ARTICLE HISTORY
Received 28 April 2023
Accepted 22 August 2023

KEYWORDS
Ag_2Se; Raman; MO dye; UV/visible light irradiation; photodegradation

Introduction

Energy utilization is promptly enhancing owing to the rapid growth of the world population and it will be almost doubled by 2050. Our energy resources are dependent upon the consumption of fossil fuels which has been accredited to raise the environmental pollution ensuing global warming.[1,2] The anthropogenic boost in environmental pollution plays a crucial role in the increasing temperature.[3,4] Recently, the world community also showed large concern regarding the abrupt growing pollution of water resources. For this purpose, a number of techniques have been put forward by the researchers from all over the globe to present suitable materials to decrease noxious pollution.[5–7] Industrial dyes, paints, pigments, and textile industries are the major cause of the water pollution. Approximately ten thousand different kinds of commercial dyes and pigments exist and approximately 7 to 8 lacs tones are produced annually worldwide. More than 75% of these are released into waters annually over industrial sewage ejections, as a consequence, it not only has adverse effects on aquatic and human health but also impacts photosynthetic process as well as dissolved oxygen concentration, hence creating severe environmental pollution.[8–10] Methyl Orange (MO), Remazol Brilliant Blue R, and Rhodamine B (RhB) are mostly used for industrials purpose. These organic dyes are easily dissolvable in water and have high toxicity. They become a main cause of dangerous diseases and are known to be teratogenic, carcinogenic or mutagenic etc.[11–19] In recent decades photocatalysis-based materials are used for the eradication of environmental problems. Semiconductor photocatalysis has unique properties, for instance they are of low-cost and are environment friendly.[20–22]

Silver selenide (Ag_2Se) n-type chalcogenide family are the most promising candidates for photocatalysis.[23,24] Ag_2Se has two stable phase structures, i.e., α-phase Ag_2Se (above 400°K) β-phase Ag_2Se with orthorhombic structure (below 400°K).[25–27]

CONTACT Asghar Ali asghar246@gmail.com Department of Physics, The University of Lahore, 1-km, Defense Road, Lahore 54000, Pakistan

Recently (Ag_2Se) has attracted considerable attention due to, its large magneto-resistance and high electrical conductivity. Owing to its outstanding properties silver selenide (Ag_2Se) was anticipated for an extensive range of applications, for example in gas sensor for carbon tetrachloride detection and in electrochemical sensor for the detection of dopamine. It is also used in non-linear optical devices, in ion-selective electrodes, in photoelectric secondary batteries, as photosensitizer and also for dye degradation.[28–30] Ag_2Se has good photodegradation properties but shows some shortcomings such as, low absorption rate in visible light, easy recombination of photoexcited e^-/h^+ pairs, and deficiency of movement constancy.[30] On the other hand, silver (Ag) belongs to noble materials that are normally cast-off in plasmonic photocatalysts owing to its outstanding plasmonic properties.[31] Here we reported a quick and simplistic method for the synthesis of Ag_2Se nanocomposite, with improved properties, through wet chemical technique.[32] The prepared nanocomposite is then examined for its photodegradation efficacy under VU/Visible light.

Experimental Section

Materials

The Silver nitrate ($AgNO_3$) powder, 99% pure selenium powder (Se), sodium borohydride $NaBH_4$, hydrogen peroxide(H_2O_2), sodium sulfite ($Na_2SO_3{\cdot}7\,H_2O$, 95%) and ammonium hydroxide (NH_4OH, 25–28%) were procured from the Korean Company "Duksan Pure Chemicals Co. Ltd.," Republic of Korea. We utilized all chemicals without any additional cleaning. All procedures were carried out with refined water.

Synthesis of Ag_2Se nanoparticle

The Ag_2Se nanoparticles were synthesized in aqueous phase by the methodology used by P.Sibiya et.al. (2014) e with minor variations.[33] The preparation of selenium precursor solution was done by adding (0.61 g-0.212 g) selenium powder to (25 mL) distilled water in a 3-necked flask, at ambient temperature. After this first reaction, mixture of $NaBH_4$ (0.9 mg) was then added. The ingredients were further mixed for 2 hours at room temperature. Later on, the preparation of starch covered silver selenide nanoparticles was done by adding (1.8 g) solution of silver nitrate $AgNO_3$ (1.4–1.8 g) to 25 mL soluble starch solution in a beaker. The mixture was repetitively mixed at room temperature. Incorporating variations in the amount of the Ag precursor is beneficial for improving reliability, understanding the structure-property relationship, and for optimizing the synthesis conditions.[34,35] Then transparent selenide ion solution was added and the resultant mixture was additionally stirred for 20 hours at room temperature. Finally, the centrifugal process was performed on the solution and the gray-black precipitates of Ag2Se nanoparticles were extracted. The precipitates were washed and dried at room temperature.

Dye degradation through artificial photo-catalysis

A wet chemical technique was used to synthesize Ag_2Se nanocomposites with photocatalytic activity via visible-light-induced dye degradation (MO as organic dyes) in aqueous media. The lamp's wavelength ranged from 400 to 790 nm, and its luminous efficacy was 80 lm/W. A dark box contained the lamp, which was placed 80 mm above the aqueous solution. During all tests, the early concentration of the dyes was fixed at 1×10^{-5} mol/L in 100 ml aqueous solution. The prepared solution was stirred on a magnetic stirrer at 20–22°C for half an hour continuously, and the reactor was transferred to a dark box for one hour to sustain the adsorption/desorption equilibrium condition of the dye. Afterwards, the system was exposed to visible light source. The samples were collected after 15, 30, 45, 60, 75, 90, 105, 120, 135 and 150 min respectively. To remove solid materials from aqueous solutions, the sample was centrifuged for 15 min. The synthesized aqueous solution was examined by a UV – vis spectrophotometer

The samples were characterized by X-ray diffraction (Pan analytical Cu k alpha) for structural analysis. The surface morphology of the composite was investigated by SEM and TEM analysis. The Raman spectra of the samples were recorded using Raman Microscope (Raman and PL set up, Renishaw UK). The transmittance, optical band gap and degradation were calculated by UV – vis spectrophotometer (Optizen POP, Mecasys Co., Ltd., Daejeon, Korea).

Results and discussions

In order to calculate the crystallographic structure of Ag_2Se nanocomposites the XRD investigation was accomplished. The Fig. 1 displays the XRD pattern of Ag_2Se (10%). In the graph the characteristic peaks appeared at various angles, including 30.7°, 33.11°, 34.6°, 36.8°, 40.0°, 39.7°, 42.3°, 43.2°, 44.9° and 48.3°. The corresponding lattice planes of the peaks are (102), (120), (112), (121), (013), (122), (201), (130), (211) and (213), respectively. The formation of Ag_2Se

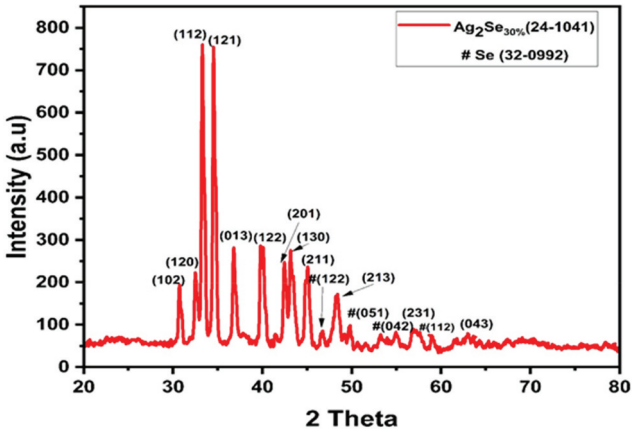

Figure 1. XRD pattern of Ag_2Se (30%).

nanocomposite is confirmed by the occurrence of these peaks. Some peaks of Se having low intensity also appeared in the XRD scan.

The full width half maxima (FWHM) of the main peaks were calculated and complied in Table 1. The crystallite size of the nanocomposite was calculated by Scherer's formula in equation 1.

$$\mathbf{D} = \mathbf{K}\lambda/\beta\mathbf{Cos}\theta \quad (1)$$

Where the value of constant K was 0.94 and $\boldsymbol{\lambda}$ presented the wavelength of X-rays. The value of $\boldsymbol{\beta}$ was taken from FWHM of the peaks and θ is the Bragg's diffraction angle. Furthermore, the dislocation density (δ) and strain (ε) of the nanoparticles were also calculated from XRD data by using following equations 2 and 3 and complied in Table 1.[36]

$$\delta = \mathbf{1}/D^2 \quad (2)$$

$$\varepsilon = \beta/\mathbf{4tan}\theta \quad (3)$$

In the above equations β and D are FWHM and crystallite size respectively.

At room temperature the selenium is amorphous [27], so by increasing the percentage of selenium by 20% (sample B) and 30% (sample C) in silver\the XRD graphs showed amorphous behavior. The XRD of sample B and C did not show any peak in the graph. Figure 2 (a, b) describes surface morphology of the prepared 30% Ag_2Se sample investigated by SEM. The synthesis of Ag_2Se nanocomposite through a wet chemical technique at a lower temperature is advantageous due to its

Table 1. The FWHM, crystallite size. Dislocation density and strain of XRD peaks.

No	Peak	FWHM	Crystallite Size (nm)	Dislocation density (10^{-12}) (m^{-2})	Strain (10^{-9})
1.	(112)	0.414	20.93	2.28	1.19
2.	(121)	0.414	21.00	2.26	1.24
3.	(013)	0.413	21.18	2.22	1.33

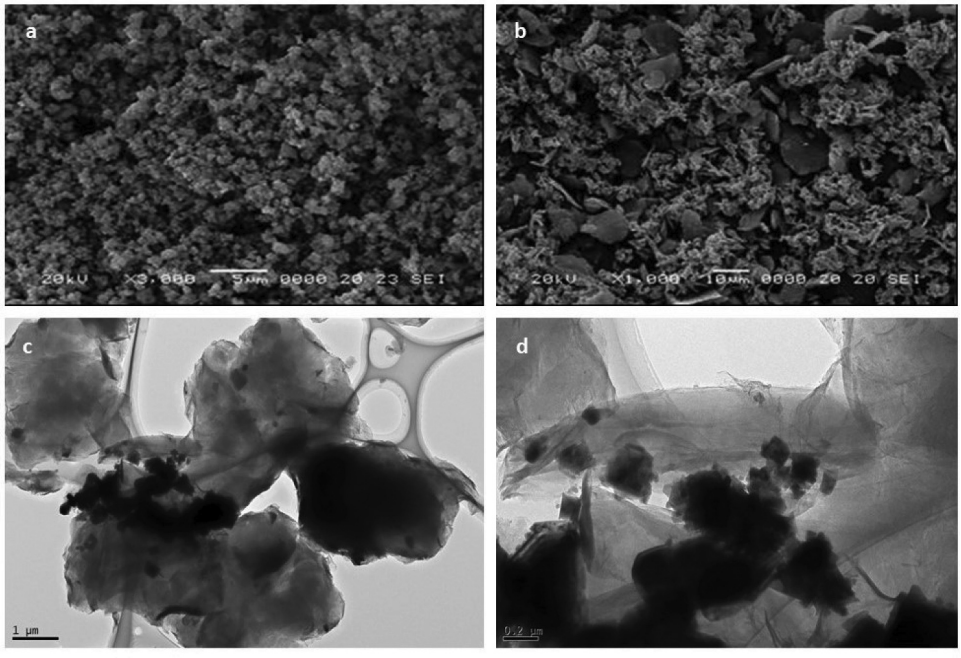

Figure 2. SEM (a-b) and TEM (c-d) images of Ag_2Se Nano-composites.

simplicity, low cost and eco-friendliness.[32,37] The Fig. 2(a, b) suggests that the Ag_2Se particles have a large surface area with a porous morphology, which is ideal for photocatalytic and dye degradation applications.[32] Fig. 2a, at a magnification of 20 kV and a resolution of 5 µm, the SEM image reveals the surface of the particles to be quite rough, with many pits and voids present. The presence of cracks in some areas suggests that the particles may not be fully dense, or may have undergone some form of mechanical deformation. In Fig. 2b, the magnification of SEM image at 10 µm resolution provide more clear details about the morphology of the particles. The irregular shape and size of the particles suggest that they have been formed by a more random and less controlled process, which can result in a higher surface area and more active sites for photo catalysis and dye degradation. Additionally, the presence of cracks and voids in the particles can provide additional surface area and potential active sites for the reaction.[37] The large surface area of the particles provides ample sites for the reaction to occur, while the cracks and voids in the particles may also provide additional active sites. The TEM image (Fig. 2c, d) with different magnification (0.1 and 0.2 µm) reveals that the Ag_2Se nanoparticles in the nanocomposite are irregularly distributed and agglomerated, forming a group of bench-like structures with an average size of 50 to 76.5 nm using image j software. The irregular shape and size of the nanoparticles suggest that they have been formed by a more random and less controlled process. This feature can result in a higher surface area and more active sites for photocatalysis and dye degradation, which is in agreement with the SEM results.

The absorption spectra of the sample recorded using lambda 750 PerkinElmer UV-visible NIR spectrometer, with the wavelength range 400–800 nm are shown in Fig 3(a–c). The samples were dispersed in DI-water to record the absorption spectra. The absorption hump recorded at 428 nm for $Ag_2Se10\%$, $Ag_2Se20\%$, and $Ag_2Se30\%$ samples was assigned to the Ag_2Se structures. The Tauc plots were obtained using Tauc equation

$$(\alpha h\nu)^2) = A(E_g - h\nu) \tag{4}$$

where α is the absorption coefficient, E_g is the band gap, h is the Planck's constant and ν is the frequency, while

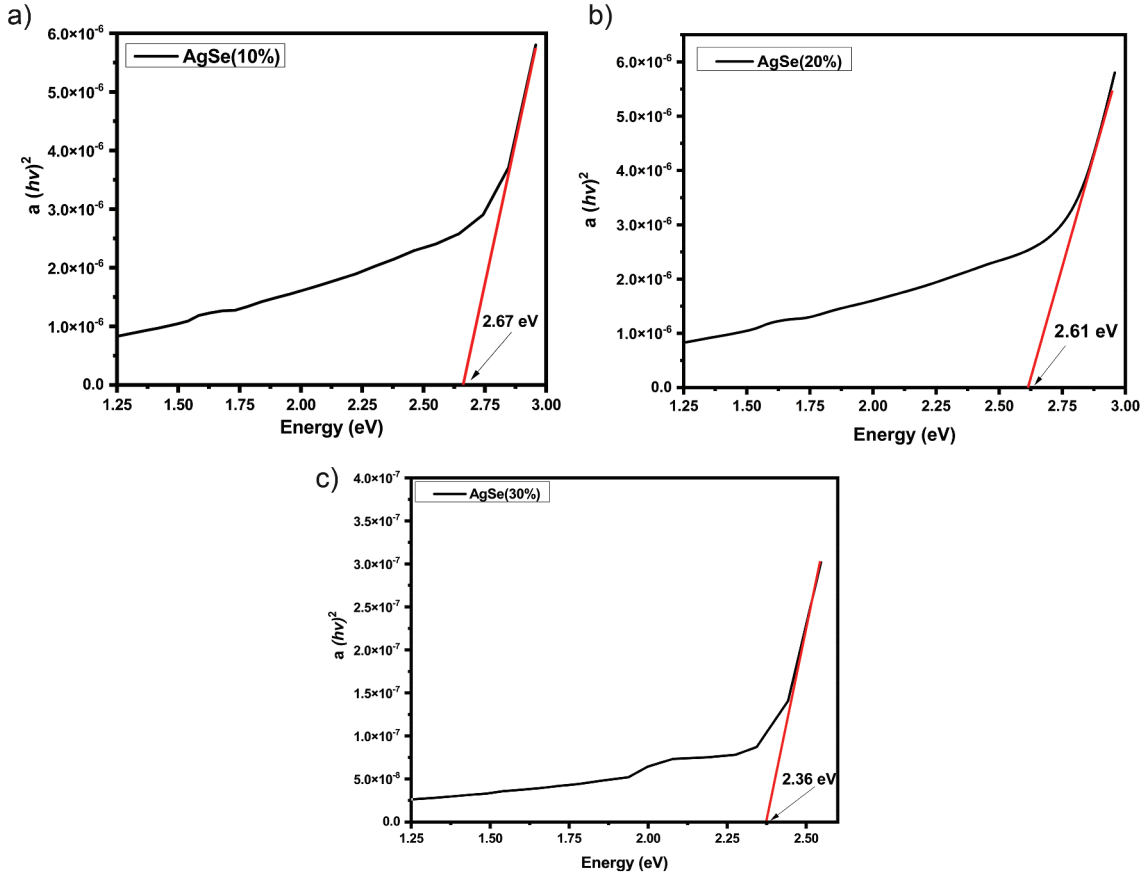

Figure 3. (A,b,c): Tuac plot of 10, 20 and 30% Se doped Ag.

A is a constant.[29] Moreover, the exponent 2 in the equation indicates direct band gap transitions, whereas the band gap of Ag_2Se could not be determined using Tauc plots.[29] The bulk structure of Ag_2Se can be assigned to effect of temperature during annealing of the samples. While the band gap calculated from the tauc plots is ascribed to be that of 2.36 eV and clearly indicates that the silver nitrate network has wider band gap and has encapsulated the lower band gap of Ag_2Se nanocomposite.

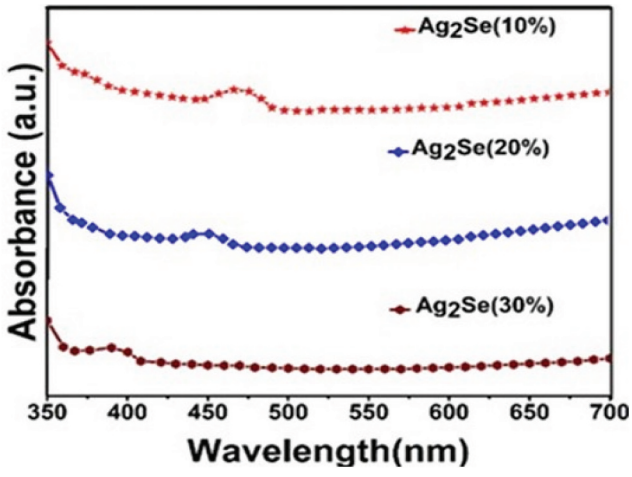

Figure 4. UV-visible NIR absorption spectra of the samples (stacked).

Figure 4 shows the absorption spectra of silver selenide nanoparticles (Ag_2Se) prepared at 10, 20 and 30% Se concentrations. The absorption spectra for all three samples exhibited an absorption shoulder at 420 nm, 470 nm and 530 nm, respectively and showed a shifted band gap from the bulk band gap of silver selenide (0.07–0.15 eV) owing toward quantum confinement. The width of the absorption shoulder increases by increasing Se percentage that could be accredited toward the self-settlement of the nanoparticles or to the development of the amorphous phase, also discussed in XRD.

The Raman spectra (Fig. 5) of the samples were recorded using Raman Microscope (Raman and PL set up, Renishaw UK) with 457 nm wavelength excitation laser. The first sample $Ag_2Se10\%$ exhibited Raman peaks of Ag_2Se at 180 cm^{-1} and 285 cm^{-1} corresponding to modes of Ag_2Se. Raman peaks of Ag_2Se 10% at 180 cm^{-2} shows the Se-Se bond and second peak positioned

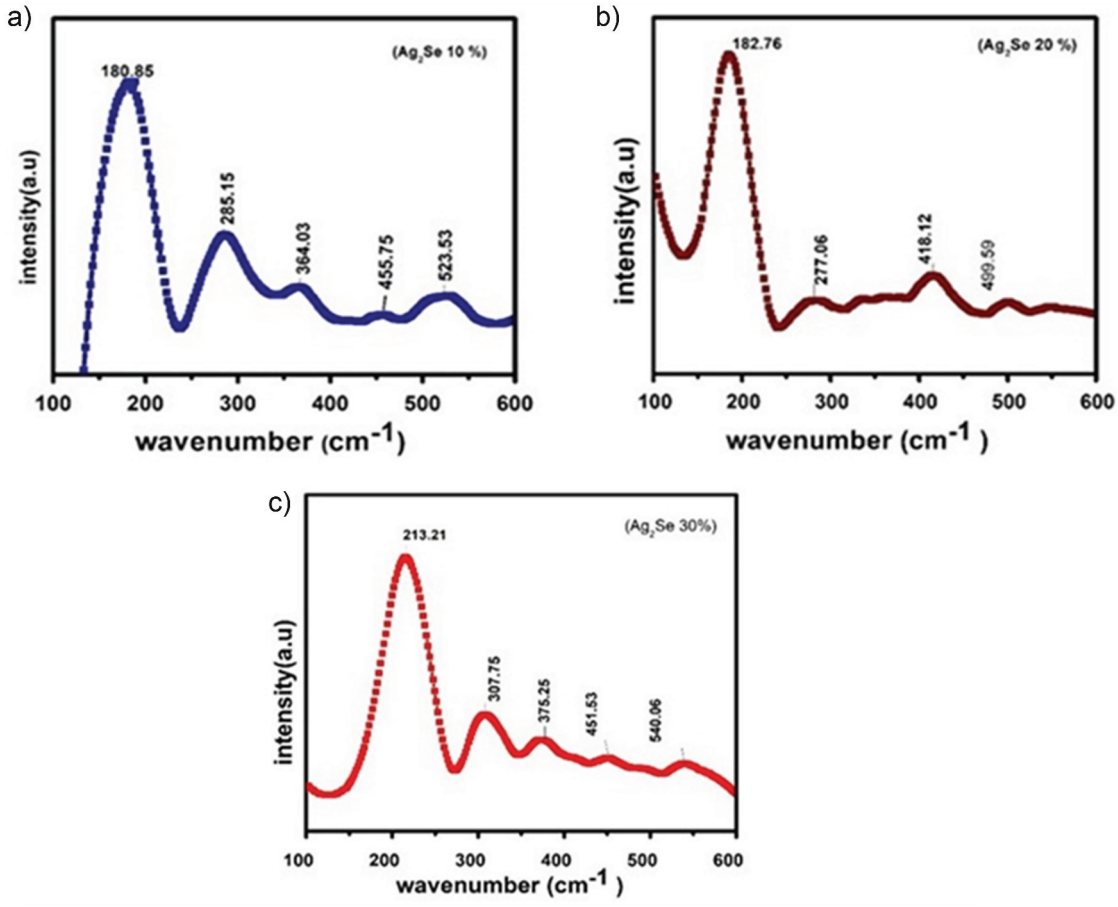

Figure 5. Raman spectra of 10,20 and 30% Se doped Ag samples.

at 285 cm^{-2} shows the Ag-Se bond while third peak positioned at 362 cm^{-2} shows the Se-O_2 bond. Raman peaks of Ag_2Se 20% at 182 cm^{-2} shows the Se-Se bond and second peak positioned at 277 cm^{-2} shows the Ag-Se bond while third peak positioned at 418 cm^{-2} shows the Se-O_2 bond. Now peak of Ag_2Se 30% at 213 cm^{-2} shows the Se-Se bond and second peak positioned at 307 cm^{-2} shows the Ag-Se bond while 375 cm^{-2} positioned third peak shows the Ag-Se bond. The details are depicted in Tables 2 and 3, i.e., absorption peak, Raman Modes, structural parameters, etc. of the prepared Ag_2Se nanocomposite.

Figure 6 shows that the transmittance improved from 25% to 80% and synthesized material can be used for optoelectronic applications. Absorbance is observed to be decreased by increasing the concentration of selenium. The graph shows the relationship between wavelength and transmittance, where wavelength is plotted on the X-axis and transmittance is plotted on the Y-axis.

Table 2. Absorption peak and band gaps of the Ag_2Se nanocomposite.

Sample	Absorption Peak	Band Gap (eV)
Ag2Se (10%)	530 nm	2.67
Ag2Se (20%)	470 nm	2.61
Ag2Se (30%)	420 nm	2.36

Table 3. Raman Modes and structural parameters of the Ag_2Se nanocomposite.

Sr No.	Samples	Peak Position	Modes
1	Ag2Se 10%	180cm^{-2}	Se-Se
		285 cm^{-2}	Ag-Se
		364 cm^{-2}	Se-O_2
		455 cm^{-2}	Se-O_2
		523 cm^{-2}	Se-O_2
2	Ag2Se-20%	182cm^{-2}	Se-Se
		277 cm^{-2}	Ag-Se
		418 cm^{-2}	Se-O_2
		497 cm^{-2}	Se-O_2
3	Ag2Se-30%	213cm^{-2}	Se-Se
		307 cm^{-2}	Ag-Se
		375 cm^{-2}	Ag-Se
		451 cm^{-2}	Se-O_2
		540 cm^{-2}	Se-O_2

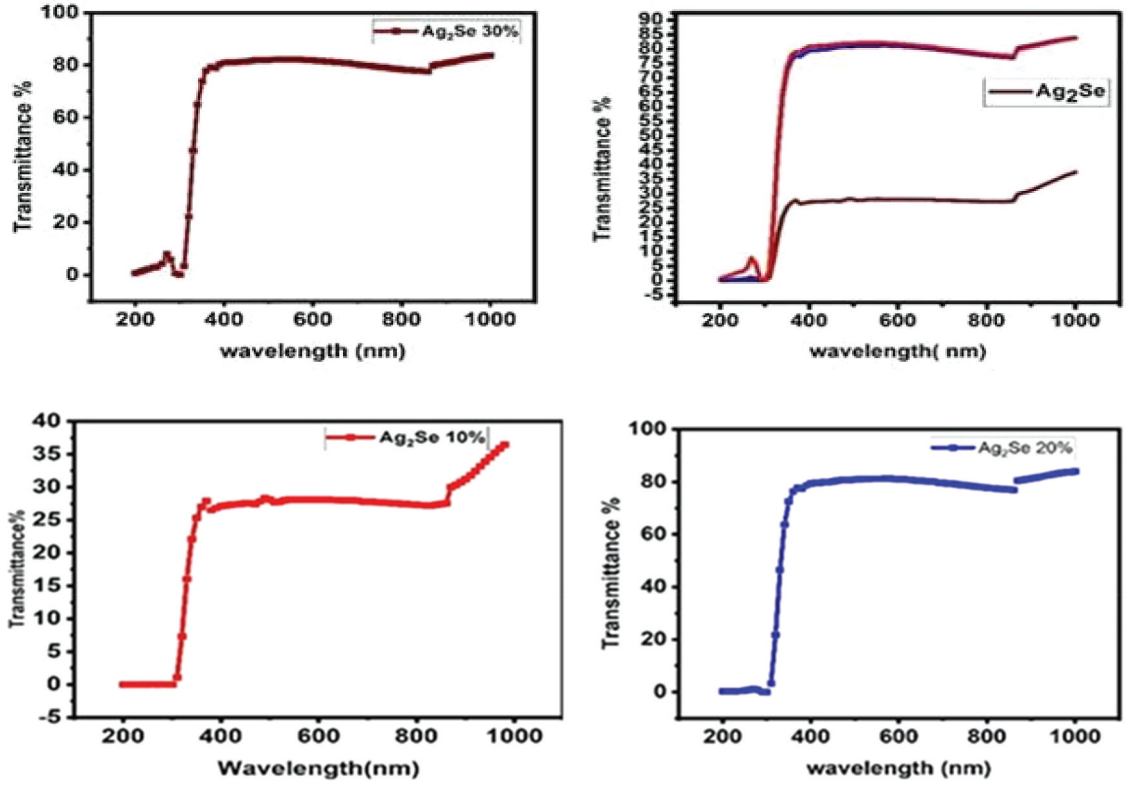

Figure 6. Transmittance data of Ag_2Se nanocomposite.

Initially for Ag_2Se 10%, as the wavelength increases, the transmittance value stays at zero as can be seen by red line in the upper left graph of Fig. 6. However, after some time, when the wavelength increases further, the transmittance value starts to increase as well. This increase continues until the transmittance value reaches 25 and then remains constant for a period of time. After this period of stability, the transmittance once again starts to increase with the increase in wavelength, this time up to a value of 950 nm. As the wavelength increases, the transmittance value increases even more, indicating a strong positive correlation between the two variables. For Ag_2Se20% (see upper right graph of Fig. 6) initially, as the wavelength increases, the transmittance value, shown by blue color, stays at zero. However, after some time, when the wavelength increases further, the transmittance value starts to increase as well. This increase continues until the transmittance value reaches 80% and then remains constant for a period of time. After this period of stability, the transmittance once again starts to show minor increase with the increase in wavelength.

The Fig. 7(a–e) shows the degradation of a MO dye using Ag_2Se 10% nanocomposites prepared via a chemical wet method, under visible light irradiation. The experiment was carried out by exposing the dye solution to the nanocomposites under visible light, and monitoring the changes in the absorbance of the solution over time. Figure 7(a–d)shows the absorbance of the dye solution at different time intervals, ranging from 0 to 150 minutes. The initial absorbance of the solution (at time 0) was 1.9329. As time progressed, the absorbance decreased, indicating that the dye was being degraded. The absorbance decreased rapidly in the first 15 minutes, and then gradually decreased over the next 135 minutes. After 150 minutes, the absorbance was found to be decreased to 0.0957. The degradation rate of the dye was calculated to be 0.015241 min^{-1}, and the half-life was 42.58 minutes. This indicates that the rate of degradation was relatively slow, but still significant. As shown in figure d, the percentage of dye degraded increased rapidly over time. After 60 minutes, more than 70% of the dye had been degraded, and after 120 minutes more than 85% while after 150 minutes 95% of the dye had been degraded. Figure e shows that the nanocomposites were stable and could be reused. The experiment was repeated four times, and the results showed that the nanocomposites maintained their effectiveness over multiple uses. The results suggest that Ag_2Se30% nanocomposites prepared via a chemical wet method can be effective for degrading MO dyes under visible light irradiation. The degradation rate is relatively slow, but still significant, and the nanocomposites are stable and can be reused multiple times.

The role of H_2O_2 in the process is as a sacrificial agent. Hydrogen peroxide is known to be an excellent oxidant and can be used as a sacrificial agent in photocatalytic reactions. When H_2O_2 is added to the system, it reacts with the photogenerated holes and produces hydroxyl radicals (•OH), which are strong oxidizing agents.[38] These hydroxyl radicals then react with the MO dye molecules and break them down into smaller, less harmful compounds such as CO_2 and H_2O. However, experiments could explore ways to increase the degradation rate and optimize the conditions for using the nanocomposites under visible light irradiation, such as adjusting the intensity or wavelength of the light source. Furthermore, the plasmonic properties of Ag arise due to conduction electron oscillation in the presence of light. The surface plasmon resonance generates the localized electromagnetic fields around the nanostructures. These concentrated fields boosted the light-matter interaction process and makes material valuable for photocatalytic applications.[31]

The overall mechanism of the photocatalytic dye degradation process involves the absorption of light by the Ag_2Se nanocomposites. This leads to the creation of electron-hole pairs, which react with oxygen and water to generate highly reactive species such as hydroxyl radicals. The degradation of dye using Ag_2Se nanocomposite as a photo catalyst with the assistance of H_2O_2 occurs through a series of steps.

Step 1. When the Ag_2Se nanocomposite is excited by photon energy, the valance band electrons (VB) move to the conduction band (CB), creating an equal number of holes in the valence band. The photo-generated electrons and holes are highly reactive and can react with a number of species. One important reaction is the combination of the electrons with dissolved oxygen to form superoxide radical anions (O_2·–). These radicals are highly reactive and can attack organic molecules, including dye molecules. The role of Ag_2Se in this step is to provide a surface for the electrons and holes to be generated on. This is important because it helps to prevent the recombination of the electrons and holes.

Step 2. The photo-generated electrons can combine with dissolved O_2 to form superoxide radical anions (O_2 ·–), while the photo-generated holes can transform HO – into HO· radical. These radicals are even more reactive than the superoxide radical anions and attack organic molecules, including the degradation of dye

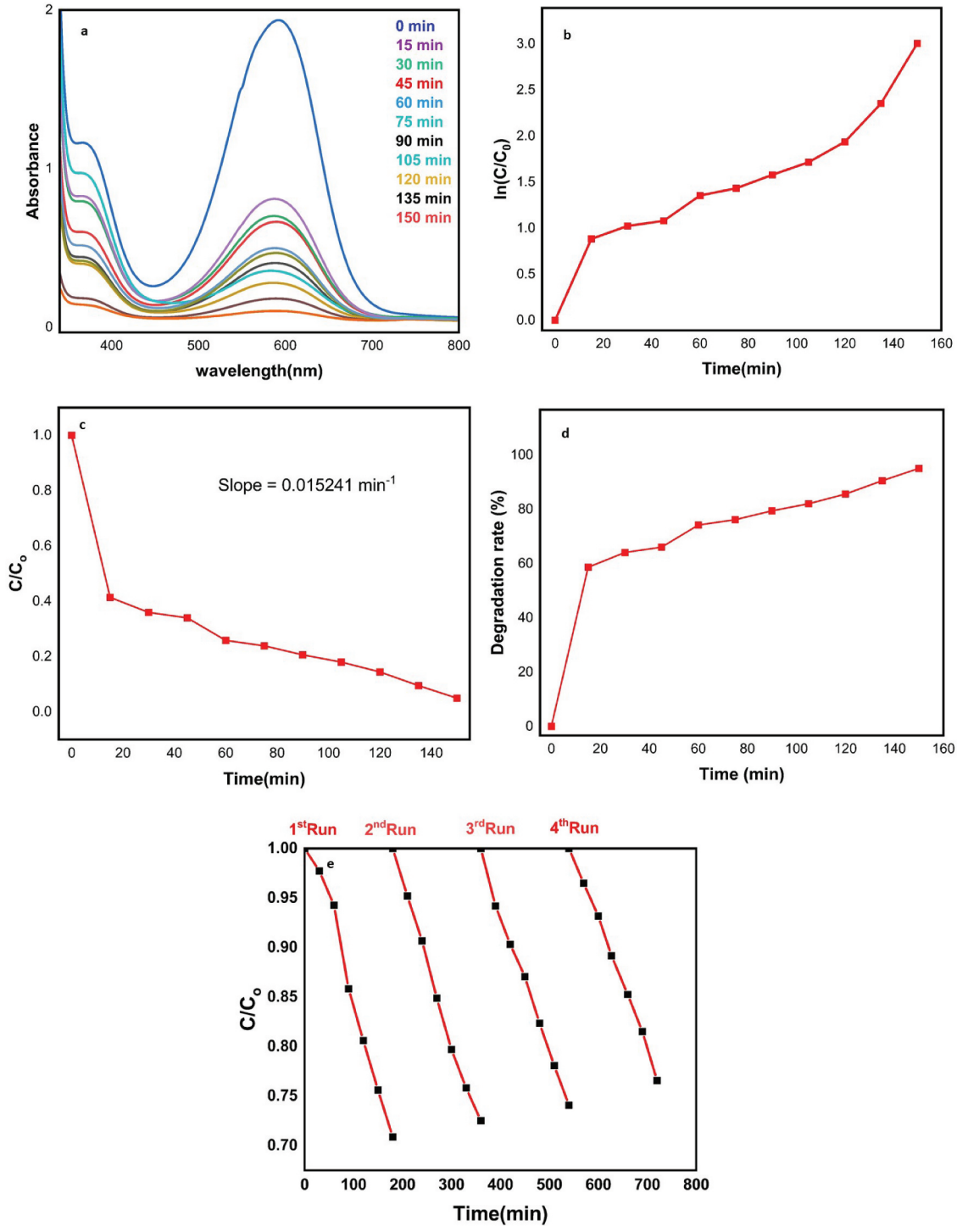

Figure 7. (a) absorbance spectra of Ag_2Se nanocomposite, (b-d) degradation kinetics, degradation rate (%) of Ag_2Se nanocomposite and (e) Recyclability of Ag_2Se nanocomposite under visible light irradiation.

molecules.[39,40] To improve the probability of photocatalytic process, the recombination of holes (h^+) and electrons (e−) needs to be minimized or the photo catalysis performance needs to be increased in the presence of a catalysts, the role of Ag_2Se nanocomposites to provide a surface for the electron and holes to be generated and prevent the recombination of the electrons and holes. So the absence of the catalyst might decrease their reactivity.[41]

Step 3. In this process, H_2O_2 plays an important role as it acts as an electron acceptor and forms hydroxyl radicals. The process involves two mechanisms: direct photolysis of H_2O_2 and the reaction between H_2O_2 and electrons. The direct photolysis of

H_2O_2 occurs after the absorption of visible light and generates free radicals, two hydroxyl radicals are produced in this process, and these radicals can subsequently interact with dye molecules. H_2O_2 can also react with electrons to produce hydroxyl radicals. This reaction is less efficient than the direct photolysis of H_2O_2, but it can still contribute to the degradation of dye molecules. Furthermore, hydroxyl radicals can be created by the reaction of H_2O_2 with electrons. Although this process is less effective than H_2O_2 being directly photolyzed, it can however contribute to the decomposition of dye molecules.[42,43] H_2O_2 is also recommended to be a better electron acceptor than oxygen, which minimizes the possibility of electron – hole recombination and generates one hydroxyl radical instead of the weaker O_2·– radical.[38]

Step 4. The hydroxyl and superoxide radical anions generated in this way create an unstable dye radical which may further decompose resulting in degraded products. The dye radical has the potential to be decomposed form degraded products. These products are typically nontoxic and can be easily eradicated from water.

Step1.

$Ag_2Se + h\nu \rightarrow Ag_2Se^*$

$Ag_2Se^* \rightarrow Ag+ + Se–$

Step 2.

$e– + O_2 \rightarrow O_2\cdot–$

$h+ + H_2O \rightarrow HO\cdot + H+$

Step 3.

$H_2O_2 + h\nu \rightarrow 2\ \cdot OH$

$H_2O_2 + e– \rightarrow \cdot OH + H+$

Step 4.

$OH + MO\ dye \rightarrow MO\ dye^*$

$MO\ dye^* \rightarrow$ Degraded products

Overall reaction

$Ag_2Se + O_2 + H_2O + MO\ \ dye \rightarrow Ag+ + Se– + O_2\cdot– + \cdot OH + H+ +$ Degraded products

Conclusion

The results of the study demonstrate the potential of Ag_2Se nanocomposites as an effective photo catalyst for dye degradation. The XRD pattern confirms the formation of Ag_2Se nanocomposites, and the SEM and TEM images show irregularly shaped particles with a rough and porous surface, which can provide ample active sites for the reaction to occur. The UV results show a shift in absorption spectra as a result of quantum confinement, and the Raman spectroscopy reveals the modes of Ag_2Se and the bonds present in the samples. The dye degradation results demonstrate a degradation rate of 0.015241 min^{-1} and a half-life of 42.58, with a high percentage of dye degradation achieved over various time intervals. The stability of the sample after multiple runs indicates the potential for practical applications. Overall, Ag_2Se nanocomposites is an efficient photo catalyst for dye degradation, with potential for wider applications in environmental remediation.

Disclosure statement

No potential conflicts of interest were reported by the author(s).

References

[1] OECD I. Energy and Air Pollution: World Energy Outlook Special Report 2016. 2016.

[2] McCollum, D.; Bauer, N.; Calvin, K.; Kitous, A.; Riahi, K. Fossil Resource and Energy Security Dynamics in Conventional and Carbon-Constrained Worlds. *Clim. Change*. 2014, *123*(3–4), 413–426. DOI: 10.1007/s10584-013-0939-5.

[3] Khatib, H. IEA World Energy Outlook 2011—A Comment. *Energy Policy*. 2012, *48*, 737–743. DOI: 10.1016/j.enpol.2012.06.007.

[4] Roy, S. C.; Varghese, O. K.; Paulose, M.; Grimes, C. A. Toward Solar Fuels: Photocatalytic Conversion of Carbon Dioxide to Hydrocarbons. *ACS Nano*. 2010, *4* (3), 1259–1278. DOI: 10.1021/nn9015423.

[5] Khan, S. B.; Irfan, S.; Lam, S. S.; Sun, X.; Chen, S. 3D Printed Nanofiltration Membrane Technology for Waste Water Distillation. *J. Water Process Eng*. 2022, *49*, 102958.

[6] Malefane, M. E.; Mafa, P. J.; Nkambule, T. T. I.; Managa, M. E.; Kuvarega, A. T. Modulation of Z-Scheme Photocatalysts for Pharmaceuticals Remediation and Pathogen Inactivation: Design Devotion, Concept Examination, and Developments. *Chem. Eng. J*. 2023, *452*, 138894. DOI: 10.1016/j.cej.2022.138894.

[7] Qiu, R.; Wang, W.; Wang, Z.; Wang, H. Advancement of Modification Engineering in Lean Methane Combustion Catalysts Based on Defect Chemistry. *Catal. Sci. Technol*. 2023, *13*(8), 2566–2584. DOI: 10.1039/D3CY00087G.

[8] Zhang, Z.; Yang, R.; Gao, Y.; Zhao, Y.; Wang, J.; Huang, L.; Guo, J.; Zhou, T.; Lu, P.; Guo, Z., et al. Novel Na2Mo4O13/α-MoO3 Hybrid Material as Highly Efficient CWAO Catalyst for Dye Degradation at Ambient Conditions. *Sci. Rep*. 2014, *4*(1), 1–9.

[9] Zhang, M.; Yang, B.; Yang, T.; Yang, Y.; Xiang, Z. A Ferric Citrate Derived Fe-NC Electrocatalyst with Stepwise Pyrolysis for Highly Efficient Oxygen Reduction Reaction. *Chin. Chem. Lett*. 2022, *33*(1), 362–367. DOI: 10.1016/j.cclet.2021.06.054.

[10] Liu, W.; Huang, F.; Liao, Y.; Zhang, J.; Ren, G.; Zhuang, Z. Treatment of CrVi-Containing Mg (OH) 2 Nanowaste. *Angewandte Chemie*. 2008, *120*(30), 5701–5704.
[11] Daneshvar, N.; Salari, D.; Khataee, A. Photocatalytic Degradation of Azo Dye Acid Red 14 in Water on ZnO as an Alternative Catalyst to TiO2. *J. Photochem. Photobiol. A Chem*. 2004, *162*(2–3), 317–322. DOI: 10.1016/S1010-6030(03)00378-2.
[12] Ledakowicz, S.; Gonera, M. Optimisation of Oxidants Dose for Combined Chemical and Biological Treatment of Textile Wastewater. *Water Res*. 1999, *33* (11), 2511–2516. DOI: 10.1016/S0043-1354(98)00494-1.
[13] Nestmann, E. R.; Douglas, G. R.; Matula, T. I.; Grant, C. E.; Kowbel, D. J. Mutagenic Activity of Rhodamine Dyes and Their Impurities as Detected by Mutation Induction in Salmonella and DNA Damage in Chinese Hamster Ovary Cells. *Cancer Res*. 1979, *39*(11), 4412–4417.
[14] Salleh, M. A. M.; Mahmoud, D. K.; Karim, W. A. W. A.; Idris, A. Cationic and Anionic Dye Adsorption by Agricultural Solid Wastes: A Comprehensive Review. *Desalination*. 2011, *280*(1–3), 1–13. DOI: 10.1016/j.desal.2011.07.019.
[15] Merouani, S.; Hamdaoui, O.; Saoudi, F.; Chiha, M.; Pétrier, C. Influence of Bicarbonate and Carbonate Ions on Sonochemical Degradation of Rhodamine B in Aqueous Phase. *J. Hazard. Mater*. 2010, *175*(1–3), 593–599. DOI: 10.1016/j.jhazmat.2009.10.046.
[16] Asl, S. M. H.; Ghadi, A.; Baei, M. S.; Javadian, H.; Maghsudi, M.; Kazemian, H. Porous Catalysts Fabricated from Coal Fly Ash as Cost-Effective Alternatives for Industrial Applications: A Review. *Fuel*. 2018, *217*, 320–342. DOI: 10.1016/j.fuel.2017.12.111.
[17] Muhmood, T.; Xia, M.; Lei, W.; Wang, F. Under Vacuum Synthesis of Type-I Heterojunction Between Red Phosphorus and Graphene Like Carbon Nitride with Enhanced Catalytic, Electrochemical and Charge Separation Ability for Photodegradation of an Acute Toxicity Category-III Compound. *Appl. Catal. B Environ*. 2018, *238*, 568–575. DOI: 10.1016/j.apcatb.2018.07.029.
[18] Muhmood, T.; Xia, M.; Lei, W.; Wang, F.; Khan, M. A. Efficient and Stable ZrO_2/Fe Modified Hollow-C_3N_4 for Photodegradation of the Herbicide MTSM. *RSC Advances*. 2017.
[19] Wan, Q.; Huang, C.-Y.; Hou, Z.-W.; Jiang, H.-J.; Wang, L. Organophotoelectrochemical Silylation Cyclization for the Synthesis of Silylated 3-CF3-2-Oxindoles. *Org. Chem. Front*. 2023, *10*(14), 3585–3590. DOI: 10.1039/D3QO00728F.
[20] Liqiang, J.; Yichun, Q.; Baiqi, W.; Shudan, L.; Baojiang, J.; Libin, Y., et al. Review of Photoluminescence Performance of Nano-Sized Semiconductor Materials and Its Relationships with Photocatalytic Activity. *Solar Energy Mater. Solar Cells*. 2006, *90*(12), 1773–1787.
[21] Pang, S.; Zhou, C.; Sun, Y.; Zhang, K.; Ye, W.; Zhao, X.; Cai, L.; Hui, B. Natural Wood-Derived Charcoal Embedded with Bimetallic Iron/Cobalt Sites to Promote Ciprofloxacin Degradation. *J. Clean. Prod*. 2023, *414*, 137569. DOI: 10.1016/j.jclepro.2023.137569.
[22] Yao, X.; Hu, X.; Cui, Y.; Huang, J.; Zhang, W.; Wang, X., et al. Effect of Mie Resonance on Photocatalytic Hydrogen Evolution Over Dye-Sensitized Hollow C-Tio2 Nanoshells Under Visible Light Irradiation. *Chin. Chem. Lett*. 2021, *32* (2), 750–754.
[23] Ma, C.; Liu, H.; Chen, R.; Su, Q.; Cui, H.; Gu, Y. Anisotropy Thermoelectric and Mechanical Property of Polycrystalline SnSe Prepared Under Different Processes. *J. Mater. Sci. Mater. Electron*. 2019, *30*(7), 6403–6410. DOI: 10.1007/s10854-019-00943-8.
[24] Jindal, S.; Singh, S.; Saini, G.; Tripathi, S. Enhanced Thermopower in (013)-Oriented Silver Selenide Films Produced by Thermal Annealing. *Appl. Phys. A*. 2020, *126*(5), 1–14. DOI: 10.1007/s00339-020-03534-1.
[25] Tveryanovich, Y. S.; Razumtcev, A. A.; Fazletdinov, T. R.; Tverjanovich, A. S.; Borisov, E. N. Fabrication of Stoichiometric Oriented Ag2Se Thin Film by Laser Ablation. *Thin. Solid Films*. 2018, *666*, 172–176. DOI: 10.1016/j.tsf.2018.09.036.
[26] Chen, R.; Xu, D.; Guo, G.; Tang, Y. Electrodeposition of Silver Selenide Thin Films from Aqueous Solutions. *J. Mater. Chem*. 2002, *12*(5), 1437–1441. DOI: 10.1039/b107177g.
[27] Jafari, M.; Salavati-Niasari, M.; Sobhani, A. Silver Selenide Nanoparticles: Synthesis, Characterisation and Effect of Preparation Conditions Under Ultrasound Radiation. *Micro Nano Lett*. 2013, *8*(9), 508–511. DOI: 10.1049/mnl.2013.0444.
[28] Ali, A.; Oh, W.-C.; Oh, W.-C.; Ali, A. Preparation of Ag 2 Se-Graphene-TiO 2 Nanocomposite and Its Photocatalytic Degradation (Rh B). *J. Korean Ceram. Soc*. 2017, *54*(5), 388–394. DOI: 10.4191/kcers.2017.54.5.03.
[29] Ali, A.; Oh, W.-C. Synthesis of $\hbox {ag}_{2}\hbox {se}$ Ag 2 Se –Graphene– $\hbox {tio}_{2} $ TiO 2 Nanocomposite and Analysis of Photocatalytic Activity of $\hbox {CO}_{2}$ CO 2 Reduction to $\hbox {ch}_{3}\hbox {OH}$ CH 3 OH. *Bull. Mater. Sci*. 2017, *40*(7), 1319–1328. DOI: 10.1007/s12034-017-1494-x.
[30] Ayele, D. W. A Facile One-Pot Synthesis and Characterization of Ag2Se Nanoparticles at Low Temperature. *Egypt. J. Basic Appl. Sci*. 2016, *3*(2), 149–154. DOI: 10.1016/j.ejbas.2016.01.002.
[31] Sayed, M.; Yu, J.; Liu, G.; Jaroniec, M. Non-Noble Plasmonic Metal-Based Photocatalysts. *Chem. Rev*. 2022, *122*(11), 10484–10537. DOI: 10.1021/acs.chemrev.1c00473.
[32] Palaporn, D.; Mongkolthanaruk, W.; S-A, T.; Kurosaki, K.; Pinitsoontorn, S. A Simple Method for Fabricating Flexible Thermoelectric Nanocomposites Based on Bacterial Cellulose Nanofiber and Ag2Se. *Appl. Phys. Lett*. 2022, *120*(7), 073901. DOI: 10.1063/5.0077137.
[33] Sibiya, P.; Moloto, M. J. Effect of Precursor Concentration and pH on the Shape and Size of Starch Capped Silver Selenide (Ag 2 Se) Nanoparticles. *Chalcogenide Lett*. 2014, *11*(11), 577–588.

[34] Wu, H.; Shi, X.-L.; Duan, J.; Liu, Q.; Chen, Z.-G. Advances in Ag2Se-Based Thermoelectrics from Materials to Applications. *Energy Environ. Sci.* 2023, *16*(5), 1870–1906. DOI: 10.1039/D3EE00378G.

[35] Haifei, W.; Chuliang, G.; Zhipeng, Z.; Qingxia, Z.; Youshi, L.; Jie, L. Chiral 1, 2-Diaminocyclohexane-α-Amino Acid-Derived Amidphos/AG (I)-Catalyzed Divergent Enantioselective 1, 3-Dipolar Cycloaddition of Azomethine Ylides. *Heterocycl.: Int. J. Rev. Commun. Heterocycl. Chem.* 2022, *104*(1), 123–139.

[36] Ansari, A. A.; Yadav, R.; Rai, S. A Facile Synthesis Approach and Impact of Shell Formation on Morphological Structure and Luminescent Properties of Aqueous Dispersible NaGdf 4: Yb/Er Upconversion Nanorods. *J. Nanopart. Res.* 2016, *18*(12), 1–12. DOI: 10.1007/s11051-016-3622-8.

[37] Glazov, V.; Pashinkin, A.; Fedorov, V. Phase Equilibria in the Cu-Se System. *Inorg. Mater.* 2000, *36*(7), 641–652. DOI: 10.1007/BF02758413.

[38] Kőrösi, L.; Prato, M.; Scarpellini, A.; Kovács, J.; Dömötör, D.; Kovács, T., et al. H2O2-Assisted Photocatalysis on Flower-Like Rutile TiO2 Nanostructures: Rapid Dye Degradation and Inactivation of Bacteria. *Appl. Surf. Sci.* 2016, *365*, 171–179. DOI: 10.1016/j.apsusc.2015.12.247.

[39] Yu, H.; Zhu, J.; Qiao, R.; Zhao, N.; Zhao, M.; Kong, L. Facile Preparation and Controllable Absorption of a Composite Based on PMo12/Ag Nanoparticles: Photodegradation Activity and Mechanism". *ChemistrySelect.* 2022, *7*(2), e202103668. DOI: 10.1002/slct.202103668.

[40] Xia, G.; Zheng, Y.; Sun, Z.; Xia, S.; Ni, Z.; Yao, J. Fabrication of ZnAl-LDH Mixed Metal-Oxide Composites for Photocatalytic Degradation of 4-Chlorophenol. *Environ. Sci. Pollut. Res.* 2022, *29* (26), 39441–39450. DOI: 10.1007/s11356-022-18989-3.

[41] Aziztyana, A. P.; Wardhani, S.; Prananto, Y. P., and Purwonugroho, D. eds. Optimisation of Methyl Orange Photodegradation Using TiO2-Zeolite Photocatalyst and H2O2 in Acid Condition. IOP Conference Series: Materials Science and Engineering, Bristol, England, UK. IOP Publishing, 2019.

[42] Wen, X.; Miao, J.; Mandler, D.; Long, M. Rotating Ring-Disk Electrode Method to Evaluate Performance of Electrocatalysts in Hydrogen Peroxide Activation via Rapid Detection of Hydroxyl Radicals. *Chem. Eng. J.* 2023, *454*, 140312. DOI: 10.1016/j.cej.2022.140312.

[43] Wan, Z.; Zhang, T.; Liu, Y.; Liu, P.; Zhang, J.; Fang, L. Enhancement of Desulfurization by Hydroxyl Ammonium Ionic Liquid Supported on Active Carbon. *Environ. Res.* 2022, *213*, 113637.